Quantum Monte Carlo simulation of a single atom interacting with an ion chain

Author: Jon López Zorrilla.
Facultat de Física, Universitat de Barcelona, Diagonal 645, 08028 Barcelona, Spain.

Advisor: Grigori Astrakharchik.
Departament de Física, Universitat Politècnica de Catalunya.
(Dated: July 16, 2019)

Abstract: The polaron concept was introduced by Lev Landau to describe a movement of an electron through the solid. Here we investigate the possibility to recreate similar physical effects in ultracold atoms, enjoying high system purity and controllability. We consider two atomic species: one is trapped in a one-dimensional optical lattice and the other is untrapped but forms molecular bound states with the first. For small, positive interspecies scattering length, the atoms form dimers but, as we increase the scattering length, the bound states overlap, allowing the untrapped atom (the "electron") to travel along the chain of trapped atoms (the "ions"). Near unitarity, the molecular forces on each ion deform their orbitals as the electron passes by, changing the electron binding energy, and forming a lattice polaron. We calculate the binding energy, distribution functions and mobility across the whole dimer-polaron crossover.

I. INTRODUCTION

During the last decades ultracold atoms have become a major research topic in physics, not only because they provide a way to study quantum effects such us Bose-Einstein condensation or superfluidity, but also because it can help study some phenomena from solid state physics. In this regard, the present work is intended to study the existence of a phenomenon similar to the electron-phonon interaction in a quantum system made of bosons. The quantum system to be simulated is an optical lattice, which resembles the usual crystalline solids, with some trapped ions and untrapped particles (impurity) acting as electrons. In particular, in this project a one-dimensional optical lattice (an ion chain) interacting with a single non-trapped impurity has been studied. Some analytical results can be found for a system like this in Ref. [1], where the ions are supposed to be pinned. Here however, no restriction will be imposed on them, except of the trapping potential. Anyway, this analytical result will be taken as a reference to check our results.

Optical lattices are usually formed by the interference of laser beams propagating in in opposite directions, leading to a periodic potential which is used to trap the ultracold atoms. The importance of optical lattices comes from two major reasons [2]. On the one had, the interference pattern can be changed to reproduce different geometries. On the other, as opposed to solids, in optical lattices the strength of the interaction between the impurity and the ions can be controlled by changing the s-wave scattering length.

Coming back to the electron-phonon interaction, one of the main features of this systems in condensed matter is the emergence of polarons. First proposed by Lev Landau in 1933 [3, 4], a polaron is a quasi-particle which originates when the ions in a solid are displaced from their equilibrium state due to the presence of the electron. One can think of it as if the electron is surrounded by the phonons, leading to a decrease of the mobility of the electron and a distortion of the lattice. Polarons have been studied in several works [5, 6], but here we pretend to study the system where polarons were first proposed by Landau: a lattice. To the best of our knowledge, this system has not been studied yet for ultracold atoms.

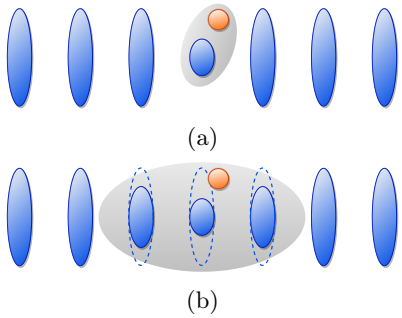

FIG. 1: (a) Dimers in the optical lattice for small scattering lengths. (b) Polaron in the optical lattice for larger scattering lengths. The orange ball denotes the impurity and the blue ellipses the oscillating ions. The shaded grey region represents the *size* of the interaction with the impurity.

We expect a similar behavior to arise in our lattice: a distortion of the ions on the chain due to the interaction with the impurity. However, a common trapping potential on optical lattices follows a pancake-like geometry, in which the ions are tightly trapped in the direction of the propagation of the chain, while the potential is softer in the transverse directions. Thus, one should not expect a longitudinal deformation of the lattice, but rather a transversal one. This effect will be studied as a function of the ratio of s-wave scattering length to the spacing between ions, as done in Ref. [1]. As in that case, two regimes are expected to appear: when the interaction scattering-length is large enough ($d/a \lesssim 1$) a polaron should be found, while for smaller lengths the impurity

is expected to form a strong bound state with a single ion. These two expected regimes are shown in FIG. 1.

Due to the quantum nature of our system, one must use proper simulation techniques in order to explore its properties. For that aim, zero-temperature Quantum Monte Carlo methods are used, which allow an *ab initio* description of the matter. Specially, the Diffusion Monte Carlo method has been widely used to study several ultra-cold atom systems [7, 8], so this is the method selected for the current project. Thus, the present work is intended not only to give some results for the chosen system, but to give some basic ideas on the computational background. In fact, a considerable time has been devoted to the understanding and implementing of the code, which this report also wants to reflect.

This report is distributed in the following way. In Sec. II the Hamiltonian of the system is introduced, giving some details on the interaction potentials chosen. Sec. III is devoted to the computational details of the project. This is probably the longest section, which pretends to provide an introduction to the quantum Monte Carlo methods used and their implementations (both serial and parallel). The computational details end with Sec. IV, where the trial wave functions needed for the calculations are shown. In the remaining sections, the results obtained during the simulations are presented. Sec. V shows the code-testing and some results for a simplified model with pinned ions. The results obtained for the whole system are explained in Sec. VI, including energies, effective mass and some qualitative discussion on the distortion of the lattice. Finally, in Sec. VII the main results and conclusions are summarized.

II. MODEL

Let us consider a system composed by N ions of mass M trapped on a potential, which interact with a different particle of mass m via a certain two body potential. The chain is chosen to propagate in the direction z, and the ions are supposed to be regularly distributed, that is, the mean distance between two neighbor ions is some constant d. This system can be modeled by the following Hamiltonian:

$$\hat{H} = -\frac{\hbar^2}{2m}\nabla_r^2 - \frac{\hbar^2}{2M}\sum_{i=1}^{N}\nabla_{R_i}^2 + \sum_{i=1}^{N}U_2(\mathbf{r},\mathbf{R}_i) + \sum_{i=1}^{N}U_1(\mathbf{R}_i), \tag{1}$$

where the first two terms stand for the kinetic energy of the particle and the ions, respectively, the third represent the interaction between the atom and the ions, and the last one models the trapping-potential for the ions.

For ultra-cold atoms the two body zero-range interaction between the atom and the ions is usually represented by delta-pseudopotential [9]:

$$U_2(\mathbf{r},\mathbf{R}_i) = g\delta(\mathbf{r}-\mathbf{R}_i)\frac{\partial}{\partial r}r. \tag{2}$$

The coupling parameter g on this equation is related to the s-wave scattering length a: $g = -4\pi\hbar^2 a/m$. This interaction, however, is not included explicitly in the energy calculation; instead, it gives rise to a boundary condition in the derivatives of the interaction wave function wave function when the distance between particle approaches 0:

$$\frac{1}{r\Psi}\frac{\partial(r\Psi)}{\partial r}\bigg|_{r\to 0} = -\frac{1}{a}, \tag{3}$$

where r is the distance between particles and Ψ the interaction wave function. This is known as the Bethe-Peierls boundary condition [10]. Therefore, this condition must be taken into account when proposing a wave function (which will be done in later sections) and, thus, the effect of the delta interaction will be included in the kinetic energy.

For a set of ions trapped in a one-dimensional optical lattice the potential can be properly modeled as an anisotropic harmonic trap, in which two frequencies are defined: one in the longitudinal direction (in the z direction) and another one in the transversal direction (defined by the plane xy).

Assuming that the i-th ion is oscillating in a trap centered on the position $\mathbf{R}_i^{(0)} = (0,0,z_i^{(0)})$, the potential energy can be expressed in the following way:

$$U_1(\mathbf{R}_i) = \frac{1}{2}M\omega_{xy}^2\left(x_i^2+y_i^2\right) + \frac{1}{2}M\omega_z^2\left(z-z_i^{(0)}\right)^2 \tag{4}$$

However, in order to check the correctness of the code developed, some calculations will be done within the Born-Oppenheimer (BO) approximations, i.e., assuming that the nuclei are static, so that there is no potential acting on them nor kinetic energy. Thus, in the BO approximation the position of the ions are fixed parameters.

Some final remarks need to be made before moving forward. The system under study is not made of fermions (as in solid state physics), but bosons. This significantly simplifies the computational implementation, since the sign problem [11, 12] appearing on fermion systems is avoided. On the other hand, even though N ions are being considered, periodic boundary conditions will be imposed in the direction of the propagation of the chain.

III. COMPUTATIONAL METHODS

The aim of this section is to briefly introduce the methods used to develop this project. As mentioned in the introduction, two different zero-temperature quantum Monte Carlo methods have been implemented: the Variational Monte Carlo (VMC) method and the Diffusion Monte Carlo (DMC) method. The first of these two is the simplest among quantum Monte Carlo methods: a trial wave function depending on a set of parameters is proposed, and the value of these parameters is optimized to give the best representation possible of the system's

ground state. Thus, the accuracy of the method is limited by the validity of proposed trial wave function. On the other hand, the Diffusion Monte Carlo method is much more sophisticated, but it allows us to overcome the limitations of the VMC and thus, the exact ground state properties can be computed.

Hence, the aim of the current section is to give some details on the basis of these algorithms and on their implementation. The VMC will be briefly discussed first, and then we will focus on the DMC method, which is more complicated both from a theoretical and a computational point of view.

A. Variational Monte Carlo

The Variational Method is based on the well known variational principle: the expected value of a given a Hamiltonian $\hat{H}$ takes its minimum value for the exact ground state wave function. The method relies on proposing an adequate trial wave function depending on a set of parameters, which we will denote α, $\Psi_\alpha(\mathbf{R};\alpha)$ and finding the optimal set of parameters that minimizes a given cost function. Usually two cost functions can be chosen: the energy or the variance (or a linear combination of them, although this has not been considered in the present work).

The most common way of proceeding is to minimize the energy, following the variational principle mentioned before. The variational energy is computed as

$$E_v(\alpha) = \frac{\int d\mathbf{R}\,|\Psi(\mathbf{R})|^2\,\Psi^{-1}(\mathbf{R})\hat{H}\Psi(\mathbf{R})}{\int d\mathbf{R}\,|\Psi(\mathbf{R})|^2}. \tag{5}$$

This integral is evaluated using Monte Carlo integration techniques, by sampling a set of M configurations $\{\mathbf{R}_i\}_{i=1}^M$ from the probability density $p(\mathbf{R}) = |\Psi(\mathbf{R})|^2$ via the Metropolis-Hastings algorithm. The energy is then estimated from this set of configurations:

$$E_v(\alpha) \approx \frac{1}{M}\sum_{i=1}^{M}\frac{\hat{H}\Psi(\mathbf{R}_i)}{\Psi(\mathbf{R}_i)}. \tag{6}$$

where $\hat{H}\Psi/\Psi$ is usually called local energy.

On the other hand, some authors defend that the variance is a better objective function to minimize [13–15], since it is positive definite and it vanishes for the exact wave ground state wave function.

In the tests done for the present project, both methods lead to similar results, so it has been decided to work with the energy minimization, which is easier to implement and interpret.

1. *Minimization method*

Since the energy (or variance) is computed from an stochastic method, there will be some statistical noise which must be avoided in the minimization process. Moreover, due to this stochastic nature, the gradient of the energy cannot be analytically computed, so the methods based on them (such as Gradient Descent or Conjugate Gradients) are hard to apply.

Several ways of overcoming these two issues have been proposed. In the present work the Simulated Annealing method has been implemented, in which no derivative are needed and the possibility of getting stuck at a local minimum is avoided. This method is motivated by the annealing done on metals; and its implementation is actually based on the Metropolis-Hastings algorithm itself. Let $F(\mathbf{x})$ be the cost function we are willing to minimize (either the energy or the variance) and T a parameter acting as an effective temperature on our system. The algorithm [16] consists on proposing a new configuration $\mathbf{x}' = \mathbf{x} + \delta\mathbf{x}$ (with some small δ random jump) and accepting it with probability

$$w_{x,x'} = \min\left(1, \exp\left\{\frac{F(\mathbf{x}') - F(\mathbf{x})}{T}\right\}\right). \tag{7}$$

The effective temperature is progressively reduced after some stabilization steps until the minimum of the cost function is found.

In our very specific case, the previous vector $\mathbf{x}$ is the set of parameters α in which our trial wave function depends.

B. Diffusion Monte Carlo

The second method used in this thesis is the Diffusion Monte Carlo method, which uses Green's functions in order to solve the time dependent Schrödinger's equation. Let us consider the imaginary-time Schrödinger's equation (where we are considering $\hbar = 1$ and $m = 1$ for simplicity):

$$-\frac{\partial\Psi(\mathbf{R},\tau)}{\partial\tau} = \left(\hat{H} - E_R\right)\Psi(\mathbf{R},\tau) \tag{8}$$

where $\tau = it$ is the imaginary time and an energy shift $\hat{H} \to \hat{H} - E_R$ has been included for convenience. Moreover, let us suppose that we know the solution of the time-independent equation, that is to say, the set of eigenfunctions $\{\Phi_n\}$ and their corresponding energies $\{E_n\}$ are known. We can expand the general solution of Eq. (8) in this basis

$$\Psi(\mathbf{R},t) = \sum_{n=0}^{\infty} c_n\Phi_n(\mathbf{R})e^{-(E_n-E_R)\tau}. \tag{9}$$

Assuming that $n = 0$ corresponds to the ground state, the energy of any other state E_n will be higher, meaning that the exponential $e^{-E_n\tau}$ will decay much faster for any of the excited states. This means that for large enough imaginary times, the last term standing in the spectral expansion is the one corresponding to the ground state.

Let us now study its asymptotic behavior for $\tau \to \infty$ depending on the energy shift introduced above. If

$E_R > E_0$, the exponent $-(E_0 - E_R) > 0$ is positive, so the wave function diverges exponentially. Contrarily, if $E_R < E_0$, the exponent is negative, so it decays to 0. Finally, if the two energies are equal $E_R = E_0$, the exponent vanishes, and the wave function converges to the ground state of the system: $\lim_{\tau\to\infty} \Psi(\mathbf{R},\tau) = c_0\Phi_0(\mathbf{R})$.

This last statement is the key element on DMC. It means that, if the shift energy is chosen to be $E_R = E_0$, for any initial state the system converges to the exact ground state when propagating it in the imaginary time [17].

Although all this is formally correct, it is not efficient from a practical point of view, since it is instable [12]. A common way to overcome the computational issues is to introduce a so called guiding or trial wave function, which is usually a wave function optimized by the Variational Monte Carlo method. The purpose of this trial wave function is to make an initial guess of the solution so that the sampling is focused on regions with larger probability.

Therefore, the wave function used up to now is replaced by a product of the trial wave function $\Psi_T(\mathbf{R})$ and the ground state wave function $\Psi(\mathbf{R},\tau)$ that we are interested in:

$$f(\mathbf{R},\tau) = \Psi_T(\mathbf{R})\Psi(\mathbf{R},\tau). \tag{10}$$

If one multiplies Eq. (8) by the trial wave function $\Psi_T(\mathbf{R})$ (and for simplicity, assuming that a single-particle system is considered), it is easy to show that the new function $f(\mathbf{R},\tau)$ satisfies the equation [18]

$$\begin{aligned} -\frac{\partial f(\mathbf{R},\tau)}{\partial\tau} =& -\frac{1}{2}\nabla^2 f(\mathbf{R},\tau) + [E_L(\mathbf{R}) - E_R]\, f(\mathbf{R},\tau) \\ &+ \frac{1}{2}\left[(\nabla\cdot\mathbf{F}) + \mathbf{F}\cdot\nabla\right] f(\mathbf{R},\tau) \end{aligned} \tag{11}$$

where

$$\mathbf{F} = 2\frac{\nabla\Psi_T(\mathbf{R})}{\Psi_T(\mathbf{R})} \tag{12}$$

is the drift force or velocity and $E_L(\mathbf{R})$ is the local energy of the trial wave function as defined in Section III A. This equation is a diffusion equation for the new wave function $f(\mathbf{R},\tau)$: the first term is the diffusion, the second stands for a branching which will be further studied in Section III B 1; and the last one acts as a drift force.

Furthermore, this interpretation of the Schrödinger's equation allows us to reinterpret the meaning of the wave function $f(\mathbf{R},\tau)$ as the probability density of diffusing particles[1]. Now we can redefine this density as a function of the population of the distribution:

$$f(\mathbf{R},\tau) = C\sum_{i=1}^{\mathcal{N}} \delta(\mathbf{R} - \mathbf{R}_i(\tau)) \tag{13}$$

where $\mathbf{R}_i(\tau)$ are the coordinates of one of the members of the population or *walkers* and C is some normalization constant. This allows us to understand the problem as a set of $\mathcal{N}$ walkers whose dynamics is governed by the diffusion equation presented above.

A formal solution to the Schrödinger's equation in Eq. (11) can be expressed in the following integral form [19]:

$$f(\mathbf{R},\tau + d\tau) = \int d\mathbf{R}'\; G(\mathbf{R}',\mathbf{R},d\tau) f(\mathbf{R}',\tau), \tag{14}$$

where $G(\mathbf{R}',\mathbf{R},d\tau)$ is the Green's function which is computed as

$$G(\mathbf{R}',\mathbf{R},\tau) = \langle\mathbf{R}'|\, e^{-\left(\hat{H}-E_R\right)\tau}\,|\mathbf{R}\rangle\,, \tag{15}$$

being $|\mathbf{R}\rangle$ a state of the position space and $\hat{H}$ the Hamiltonian acting describing the diffusion equation in Eq. (11).

However in general this Green's function cannot be computed analytically, so the main issue now is to give a valid approximation to it. On the following sections three ways of approximating the Green's function are proposed, each of the leading us to a different algorithm.

1. *Linear Diffusion Monte Carlo*

The Hamiltonian is usually split in two pieces, one corresponding to a diffusion and drift term

$$\hat{H}_1 = \frac{1}{2}\nabla^2 - \frac{1}{2}\left[(\nabla\cdot\mathbf{F}) + \mathbf{F}\cdot\nabla\right] \tag{16}$$

and a second one acting as a branching term

$$\hat{H}_2 = E_L(\mathbf{R}) - E_R. \tag{17}$$

Then, the exponential appearing in the Green's Function can be decomposed using the Baker-Campbell-Hausdorff formula, and, in this simples algorithm, the expansion is truncated neglecting the commutator between the Hamiltonians. Thus, the Green's function is split into two independent contributions:

$$\begin{aligned} G_1(\mathbf{R}',\mathbf{R},d\tau) = \langle\mathbf{R}'|\, e^{-\hat{H}_1\tau}\,|\mathbf{R}\rangle = \\ (4\pi D\Delta\tau)^{-3N/2}\exp\left\{-\frac{(\mathbf{R}' - \mathbf{R} - D\Delta\tau\mathbf{F}(\mathbf{R}))^2}{4D\Delta\tau}\right\} \end{aligned} \tag{18}$$

and

$$\begin{aligned} G_2(\mathbf{R}',\mathbf{R},d\tau) = \langle\mathbf{R}'|\, e^{-\hat{H}_2\tau}\,|\mathbf{R}\rangle = \\ \exp\left\{-\tau\left(\frac{1}{2}E_L(\mathbf{R}') + \frac{1}{2}E_L(\mathbf{R}) - E_R\right)\right\} \end{aligned} \tag{19}$$

[1] For this interpretation as a probability density to be correct, we need the distribution function to be definite positive. Since we are working with the ground state of bosons, this requirement is satisfied and the interpretation is valid.

This decomposition depends on the time step $d\tau$, and it is valid up to linear order. In practice, this decomposition works as follows [11]:

1. A new configuration $\mathbf{R}'$ is proposed where both the diffusion and the drift are included:

$$\mathbf{R}' = \mathbf{R} + \frac{1}{2}\tau\mathbf{F}(\mathbf{R}) + \xi, \tag{20}$$

   where ξ is a Gaussian random number of mean 0 and standard deviation $\sigma = \sqrt{\tau/2}$.

2. The second part of the Hamiltonian can be interpreted as the weight of each walker: the less the energy of a walker, the bigger its weight. In practice, instead of giving each walker a weight, they are duplicated following that weight. The branching factor

$$P_B = \exp\left\{-\tau\left(\frac{1}{2}E_L(\mathbf{R}') + \frac{1}{2}E_L(\mathbf{R}) - E_R\right)\right\} \tag{21}$$

   determines the number of replicas of each of the walkers, which is determined as

$$n = \text{int}(P_B + u) \tag{22}$$

   where u is a uniformly distributed random number between 0 and 1.

This branching clearly shows the purpose of the reference energy: adjusting it allows us to control the number of walkers alive. Among the several ways proposed in the literature for computing this reference energy [20], here we have chosen one of the standards:

$$E_R = \frac{1}{\mathcal{N}_j}\sum_{i=1}^{\mathcal{N}_j} E_L^{(i)} + \frac{g}{d\tau}\ln\left(\frac{\mathcal{N}_0}{\mathcal{N}_j}\right) \tag{23}$$

where $\mathcal{N}_j$ is the amount of alive walkers in the jth time step and g a parameter that must be adjusted. In our case, $g = d\tau$ has worked properly.

2. *Metropolis Diffusion Monte Carlo*

It can been shown that the previous algorithm does not satisfy detailed balance [11], which introduces a large bias in the simulation, making it necessary to take a small time step $d\tau$ to have a reasonable result. A way to impose the detailed balance on the Green's function, and thus reduce the dependence on the time step, is to add a rejection step to the previous algorithm. A move from $\mathbf{R}$ to $\mathbf{R}'$ is accepted with probability

$$P(\mathbf{R}', \mathbf{R}) = \min\left(1, \frac{G(\mathbf{R}, \mathbf{R}', d\tau)}{G(\mathbf{R}', \mathbf{R}, d\tau)}\frac{|\Psi(\mathbf{R}')|^2}{|\Psi(\mathbf{R})|^2}\right) \tag{24}$$

where $G(\mathbf{R}', \mathbf{R}, d\tau) = G_1(\mathbf{R}', \mathbf{R}, d\tau)G_2(\mathbf{R}', \mathbf{R}, d\tau)$ is the product of the two Green's functions defined in the LDMC algorithm.

Since rejection step reminds us of the Metropolis-Hastings algorithm, this second algorithm is usually called *Metropolis-Diffusion Monte Carlo* in the literature. Although this method should decrease the bias, having a smaller dependence on the time step, it has its basis on the decomposition on Eq. (18) and (19) which is only valid up to a linear order, so the dependence of the method is still linear on the time step.

3. *Quadratic Diffusion Monte Carlo*

The last method to be tried is the so called *Quadratic Diffusion Monte Carlo*, in which the Green's function's decomposition is done up to quadratic order on the time step. Although this decomposition is not unique [21, 22], all of them give this quadratic dependence. The choice taken in this work leads to the following algorithm:

$$\mathbf{R}_1 = \mathbf{R} + \sqrt{d\tau/2}\xi \tag{25}$$

$$\mathbf{R}_2 = \mathbf{R}_1 + \frac{1}{4}d\tau\mathbf{F}(\mathbf{R}_1) \tag{26}$$

$$\mathbf{R}' = \mathbf{R}_1 + \frac{1}{2}d\tau\mathbf{F}(\mathbf{R}_2) + \sqrt{d\tau/2}\xi' \tag{27}$$

where ξ and ξ' are two Gaussian random numbers with 0 mean and unit standard deviation.

4. *Algorithm*

The main parameters to be defined in the simulation are the mean number of walkers $\mathcal{N}_0$, the imaginary time step $d\tau$ and the total number of steps wanted. The use of all the formulae described in the previous sections are applied in the computational algorithm as follows:

1. **Initialization of the system**. The first step is to initialize a set of $\mathcal{N}_0$ walkers sampled from the trial distribution $|\Psi_T(\mathbf{R})|^2$ using the conventional Metropolis-Hastings algorithm. The reference energy E_T is then initialized as the mean value over all the workers of the local energy:

$$E_R = \langle E_L\rangle = \frac{1}{\mathcal{N}_0}\sum_{i=1}^{\mathcal{N}_0} E_L^{(i)} \tag{28}$$

2. **DMC time step**. For each of the walkers, a new configuration is proposed using one of the methods explained before.

   Once the new configuration has been decided, the branching factor is computed and the walkers are replicated or killed according to it: if $m = 0$, the system is deleted; if $m = 1$ the system remains untouched: and if $m > 1$, $m-1$ copies of the system are created, each of them being a new walker for the following iterations.

For the new population the local energy and the number of walkers are updated, and consequently, the new threshold energy E_R is computed.

This step 2 is repeated until the calculation is converged and the desired statistics are done. This sequence of instructions is summarized in the scheme of Figure 2.

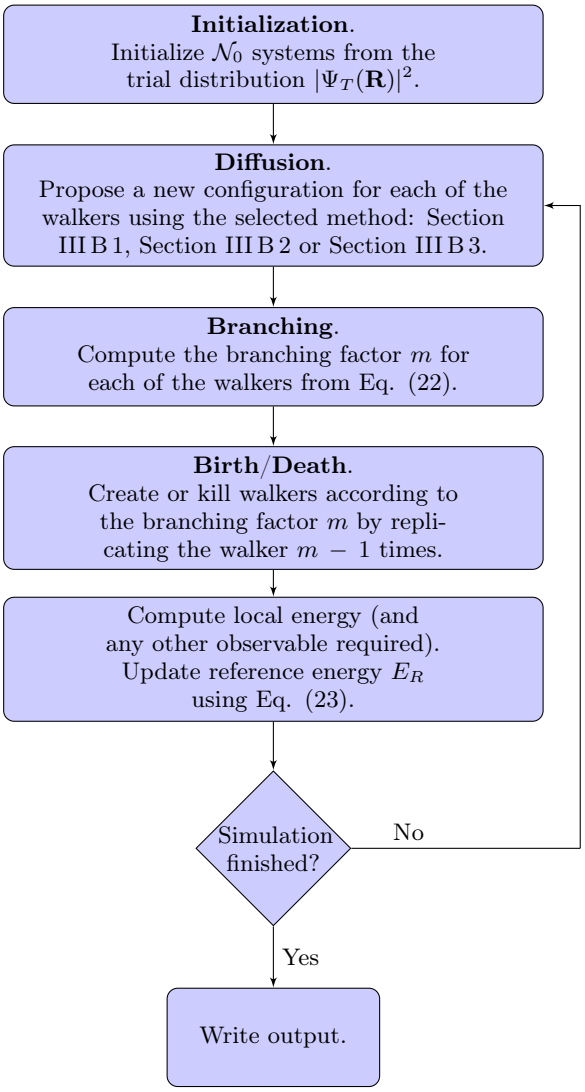

FIG. 2: Scheme of the DMC algorithm.

C. Implementation

Both the Variational and Diffusion Monte Carlo methods have been implemented in Fortran 90[2] using serial programming, as well as parallel computing using Open MPI. The implementation of the former follows the details given during this whole section, while the latter requires some more details.

The benefit of parallel programing for the VMC method is that it allows us to get better statistics. Since a Markov process is being simulated, the evolution of a single system cannot be parallelized (each new configuration depends on the previous one, so the sampling must be done in serial). However, one can simulate $\mathcal{N}$ copies of the system independently and use the configurations sampled on each system to compute the observables. Thus, its implementation is straight forward, since the only communication needed is to collect the sampled observables at the end of the simulation.

The parallelization of the DMC algorithm is more complicated: the total number of walkers $\mathcal{N}$ are divided among the processors, but this time the amount of walkers is not fixed. Due to the branching, even if the initial distribution of walkers is homogeneous, they will end up not being equally distributed, which would make the implementation inefficient. Moreover, the total energy of the system and the total number of workers need to be known at each time step so that the reference energy can be updated.

The solution to both these issues is the following leads to the need of a communication after every step. At each step every worker updates the position of their walkers, applies the branching (deleting or replicating some walkers) and computes the local energy of the walkers it is working with. Then each walker communicates the number of (local) walkers alive, and the new ideally homogeneous distribution is computed. In the last step the workers with more walkers than the average must pass them to the workers with less walkers.

Although no more information on the algorithm will be given, this exchange of walkers is done by means of the MPI_AllGather() function following the idea proposed on Ref. [23]: each worker creates a *local array* with their extra walkers, and then they all share their local arrays, so that all the extra walkers are now known by every worker. Thus, the workers with less walkers take the walkers from this shared-local-array.

IV. TRIAL WAVE FUNCTION

One last key factor which has been ignored up to this point is the construction of the trial wave function. Although in general it requires some physical intuition and knowledge of the system, there are some typical structures that are usually used for boson systems. The so called Bijl-Jastrow wave function decomposes the total wave function as a product of one-body and two-body wave functions

$$\Psi(\mathbf{r}_1,\dots,\mathbf{r}_N)=\prod_{i=1}^{N} f_1(\mathbf{r}_i)\prod_{j=1}^{N}\prod_{k>j}^{N} f_2(|\mathbf{r}_j-\mathbf{r}_k|) \qquad (29)$$

[2] The main code written for this project is accessible in the following GitHub repository: https://github.com/jlopez141/TFM.

which is indeed symmetric with respect to the exchange of two of the particles. The one body term stands for the effect external potential, while the two body term describes the interactions between particles. Of course, the functional form of the interaction functions depends on the system under study.

In our specific case, however, the trial function can be further simplified, since the particles are split in two sets: the N ions (denoted by capital letters) and the single particle acting as the impurity (lower case letter). In this scenario, there is no external potential acting on the impurity nor two body interactions between ions, so the general form of the trial wave function is reduced to the following:

$$\Psi(\mathbf{r}, \mathbf{R}_1, \dots \mathbf{R}_N) = \prod_{i=1}^{N} f_1(\mathbf{R}_i) \prod_{i=1}^{N} f_2(|\mathbf{r} - \mathbf{R_i}|). \quad (30)$$

Once the form of the trial wave function is chosen, we need to compute its first and second derivatives, in order to compute the drift force and the local kinetic energy, respectively.

A. One body wave function for an anisotropic harmonic trap

It there were no particle, the solution to this potential would be a Gaussian, so that is the trial wave function proposed for the ions. However, the exponents of the Gaussian are left as variational parameters to account for the effect of the particle.

$$f_1(\mathbf{R}_i) = \exp\left\{-\alpha_{xy}\left(x^2 + y^2\right) + \alpha_z\left(z - z_i^{(0)}\right)^2\right\}. \quad (31)$$

B. Two body wave function for δ-pseudopotential interaction

The two body interaction is decomposed as follows:

$$f_1(r) = \begin{cases} \frac{1}{r}\exp\left\{A - \frac{r}{a} - Br^2 + Cr^3\right\} & , r \leq R_p \\ 1 & , R_p < r < L/2 \end{cases} \quad (32)$$

which can be shown to fulfill the Bethe-Perierls boundary condition in the $r \to 0$ limit. Here the parameters B and R_p are variational parameters to be adjusted, while the remaining two parameters are chosen to ensure that the wave function is continuous and differentiable at $r = R_p$.

The function is chosen to smoothly approach 1 for a distance $L/2$ so that periodic boundary conditions can be imposed. In fact, the variational parameter R_p determines the size of the interaction, and could be interpreted as a correlation length between ions and impurity. Thus, it must be $R_p < L/2$ so as to avoid the double counting on the interaction with the ions due to periodic boundary conditions.

V. PRELIMINARY STUDY

A. Methodological Aspects

The first step given in order to check the correctness of the code is to simulate the chain with pinned ions, for which the exact result is known. Thus, the three implementations of the DMC algorithm can be confronted with the analytical result.

These preliminary simulations have been done using a chain with $N = 10$ ions separated by a distance of $d = 10$ and for a scattering length of $d/a = 2$. The reader should notice that even if only 10 ions are considered, periodic boundary conditions are imposed in the direction of the propagation of the chain, so an infinite chain is being studied. The results for the three methods proposed during the theoretical analysis (standard DMC, Metropolis DMC and quadratic DMC) are shown in FIG 3.

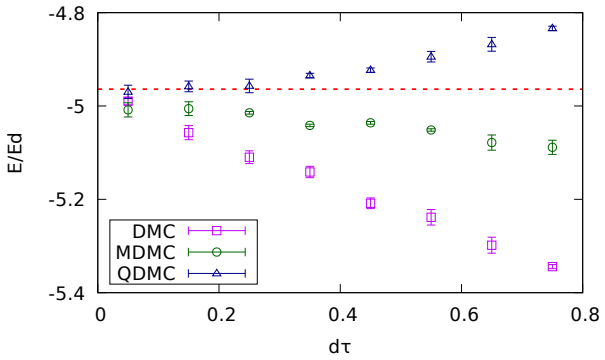

FIG. 3: Energy as a function of the time step for the three DMC implementations for $d/a = 2$. The red dashed line shows the exact energy.

As expected, both DMC and MDMC scale linearly, but the Metropolis-like rejection step significantly reduces the bias. On the other hand, the behavior of QDMC is quadratic with the time step. In light of these results, it is clear that the scaling fits the expectations. In view of the results, it has been decided to work with the MDMC implementation.

As a final remark, it must be said that the choice of the scattering length $d/a = 2$ is arbitrary, and a similar behavior can be observed for any other value.

On the other hand, the efficiency of the parallel code must be tested. For that purpose, the simulations have been carried out for the whole system (with mobile nuclei), since it is the system that we are interested in studying. As in the previous test, $N = 10$ mobile ions have been simulated with the same equilibrium distance $d = 10$ and for a scattering length $d/a = 2$.

Both the variational and diffusion Monte Carlo algorithms have been tested. In the first the population is fixed in $\mathcal{N}_0 = 500$, while in the latter the mean value of the walker population is chosen to be $\mathcal{N}_0 = 500$. In both

cases 10^6 steps have been given[3].

In order to check the efficiency of the implementation two magnitudes have been defined: the speedup and the efficiency itself. The speedup is defined as the time ratio of the computation using a single processor and using P of them. For an ideal division of the work, the speedup should be linear with the number of processors. The efficiency is then defined as the speedup divided by the number of processors, which ideally should be the unit for any number of processors.

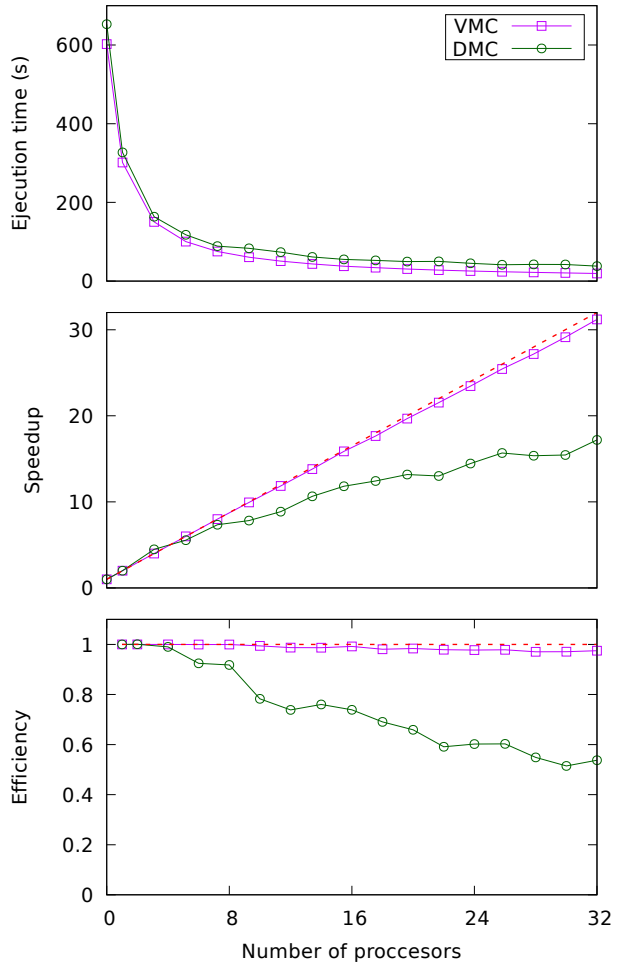

FIG. 4: Execution time, speedup and efficiency of the VMC and DMC parallel implementations in a run of 10^6 time steps with $\mathcal{N}_0 = 500$ walkers. The red dashed line shows the ideal behavior.

FIG. 4 shows the scaling of both methods. As expected, the Variational method scales almost as if it were ideal, due to the lack of communications between workers. On the other hand, the DMC implementation is much further from being ideal. This was expected as well, since many communications must be done this time.

B. Born-Oppenheimer Approximation

Before starting to study the system with mobile ions, it has been decided to replicate the analytic results known for pinned ions (computed within the Born-Oppenheimer approximation). This should provide some physical insight of the system under study and help us understand the rest of the results. Moreover, this can help us compare the VMC and DMC methods too.

The first observable to be computed is the energy of the impurity as a function of the s-wave scattering length. The computational results are compared to the analytical form of the energy derived in Ref. [1]:

$$E(k) = -E_d \text{arccosh}^2\left(\frac{e^{d/a}}{2} + \cos kd\right) \tag{33}$$

where $E_d = \hbar^2/2md^2$ is the recoil energy and $\hbar k$ is the momentum of the impurity (our calculations correspond to a nil momentum).

The results in FIG. 5 show that the VMC method gives an upper bound to the energy (following the variational principle), while the DMC results lay on top of the exact result (so it is exact within the statistical error). Therefore, from now onwards the variational method will be put aside, and we will only show the results of DMC. Of course, VMC will still be used to provide a first approximation for the DMC guiding wave function.

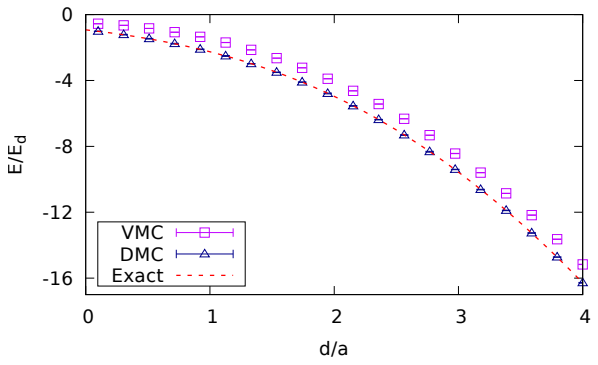

FIG. 5: VMC and DMC energies for pinned ions. The errorbars are so small that can barely be seen.

Moreover, the band-mass of the impurity can be computed for the Born-Oppenheimer approximation, both analytically and computationally. The analytical results can be easily derived from the energy, following the usual

[3] These VMC calculations do not consist in optimizing the parameters, but rather computing the energy for a given set of parameters.

steps from solid state physics:

$$\frac{m}{m^*} = \frac{1}{\hbar^2}\left.\frac{\partial^2 E}{\partial k^2}\right|_{k\to 0} = \frac{\operatorname{arccosh}\left(e^{d/a}/2+1\right)}{\sqrt{e^{d/a}+\frac{1}{4}e^{2d/a}}}. \tag{34}$$

On the other hand, the effective mass can be computed from the DMC calculations using the following dispersion relation between the mean square displacement along the z direction and the imaginary time τ:

$$\left\langle (\Delta z(\tau))^2 \right\rangle = \frac{\hbar^2}{2m_{\text{eff}}}\tau \tag{35}$$

where $\langle\cdot\rangle$ denotes the average over all the walkers that are alive at the end of the simulation.

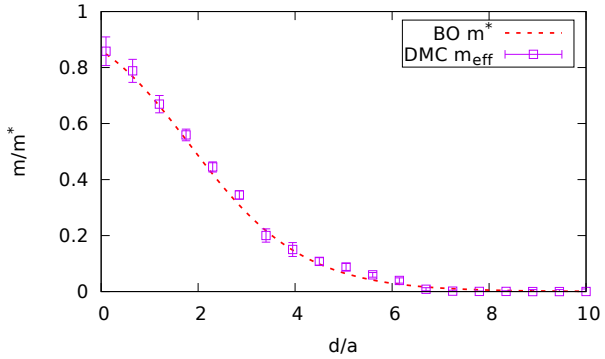

FIG. 6: Band mass (red dashed line) and effective mass (black cross) of the impurity in the chain.

The results shown in Fig. 6 show that the diffusive effective mass is actually the same magnitude as the band-mass computed from the energy. This is something to be taken into account when studying the system with mobile ions.

VI. RESULTS

The main objective of the present project is to study the how the system changes when letting the ions move, which will be studied in this last section. As in the previous section, the number of ions in the system is $N = 10$ with $d = 10$ and imposing periodic boundary conditions. The Diffusion Monte Carlo algorithm has been employed to perform every simulation in this section. The mass of the ions has been chosen the same as the one of the impurity.

A. Stability diagram

The first feature that can be observed in this system is the possibility of collapsing: if the interaction between the particle and the nuclei is strong enough, the particle can create a strong bound-state with more than one these nuclei, so that the ions are forced out of their equilibrium position and are pulled together. The condition for this to happen can be such that the energy due to the bound state is of the order of the energy of the harmonic trap. These energies are, respectively:

$$E_b = -\frac{\hbar^2}{2\mu a^2} \tag{36}$$

$$E_\omega = \frac{1}{2}\hbar\omega = \frac{\hbar^2}{2Ma_\omega^2} \tag{37}$$

where $a_\omega = \sqrt{\hbar/M\omega}$ is the typical length scale of the harmonic oscillator and μ is the reduced mass of the ion-particle couple. Here we have only considered the energy due to the trap in the direction of the propagation of the chain, which is the only direction in which the collapse can happen. Equaling this two magnitudes, we can estimate for which value of the scattering length should the collapse occur:

$$E_\omega \sim |E_{\text{bound}}| \Longrightarrow \frac{a_\omega}{a} \sim \sqrt{\frac{\mu}{M}} = \frac{1}{\sqrt{1+M/m}} \tag{38}$$

This theoretical limit is confronted with the computational result in FIG. 7. The number of collapsed ions shown in that figure is determined by counting how many ions are in a small region around the particle ($|\mathbf{r}-\mathbf{R}_i| \lesssim 0.1d$), which is averaged for the whole simulation time. Although our prediction is not exact, this result clearly show that there are two separated regimes.

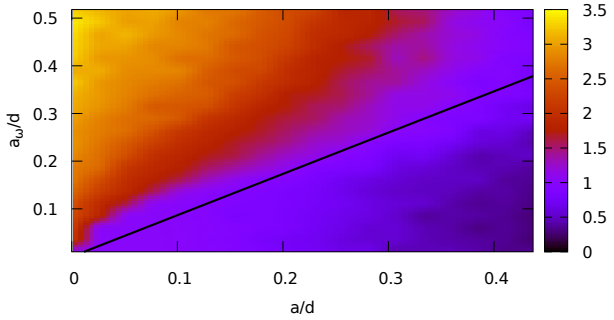

FIG. 7: Stability diagram for $M/m = 1$. The color legend shows the average number of collapsed ions.

However, this phenomenon is not thought to be physical, since the collapsed regime is governed by three or more body bound states, and our model does not include any kind of ion-ion interactions. In fact, if one included the repulsive interaction between ions the collapse would not happen. Anyway, in regards to our model, the collapsing delimits a zone in which our calculations are not valid.

In order to avoid this forbidden regime, one should take a small enough oscillator length in the z direction (the x and y directions are not affected by this phenomenon,

since the chain is only periodic in the z direction). In view of the results, taking $a_z = 0.1d$ seems a good choice, which ensures stability up to $d/a \sim 10$.

B. Distortion of the lattice

In the following sections we intend to explore the existence of polarons in the ion chain. A possible choice of parameters to avoid the collapse is $a_x = a_y = d$ and $a_z = d/10$ with the scattering length a changed in a wide range.

It is expected that some distortion occurs to the ions due to the interaction with the particle. The main issue is what observable to choose in order to prove it. On the one hand, since we want to observe the distortion of the ions, the ion-ion two body correlation function seems to be the appropriate one. However, the effect of the impurity should be relevant only for a few of the ions, while the correlation function includes every of them. Therefore, the distortion would be hard to distinguish from this observable.

Finally, the selected observable is a projection of the particle-ion density, computed as follows: at every time step, the relative position vector $\mathbf{u}_i = \mathbf{r} - \mathbf{R}_i$ is computed for each of the nuclei. The z axis shown in the figure stands for the z component of this relative vector, while the x/y axis shows the x and y components (so that we are taking advantage of the cylindrical symmetry). This basically provides the configuration of the system from the particle's reference system.

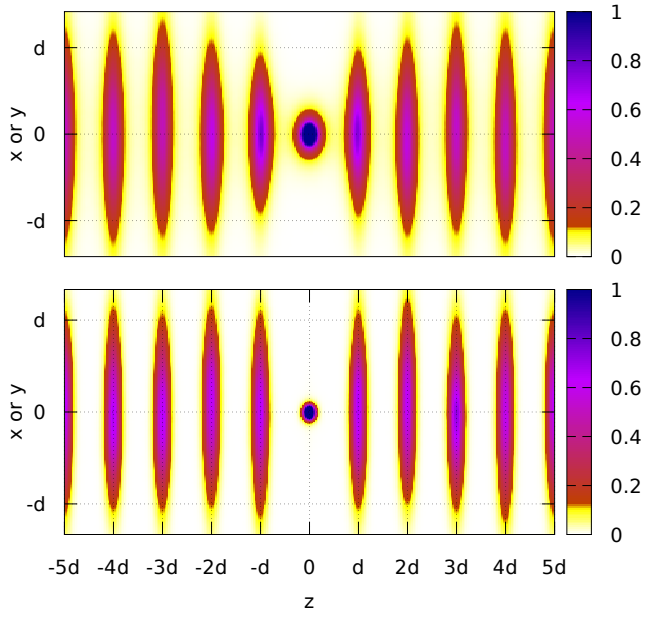

FIG. 8: Distortion of the ions in the lattice. Top: $d/a = 1$. Bottom: $d/a = 10$.

The results obtained are shown in FIG. 8 for two different scattering lengths, which show different behaviors. On the one hand, for a large scattering length ($d/a = 1$), there is indeed a transversal distortion on the lattice due to the presence of the impurity, not only for the nearest ion, but for many of them. This seems to correspond to a polaron. On the other hand, when decreasing the scattering length ($d/a = 10$), so does the correlation length between the ions and the impurity, which finally leads to the localization of the particle around a single ion. Thus, the ion and the impurity are strongly bounded making a dimer while the rest of them are unaffected.

C. Effective mass

Even thought this result seems to mean that there are two regimes (polaron and dimer) it does not seem enough to state that it is indeed a polaron. The previous result shows that there is a distortion due to the presence of the impurity, but this must propagate along the chain for it to be a polaron. So as to prove it, we will proceed to compute the effective mass of the particle in the ion chain.

The effective mass of the particle has been computed as done in the preliminary calculations for the pinned ions. This result, along with the ones obtained for the BO approximation, are shown in FIG. 9.

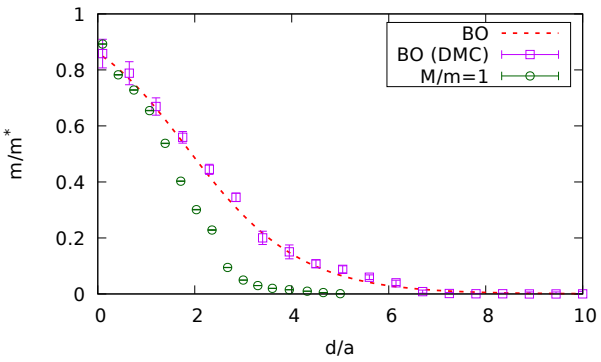

FIG. 9: Band mass (red dashed line) and effective mass (black cross) for the Born-Oppenheimer approximation; and effective mass for $M/m = 1$ mass ratio.

This mass can be interpreted in terms of its mobility, a finite mass meaning that it is mobile so it can propagate. In view of this result, it has been proved the existence of the polaron: for large scattering lengths, small d/a, there is a finite mass (polaron), while it becomes infinite for small scattering lengths, meaning that it does not propagate anymore (dimer regime).

Compared to the BO approximation, the main change introduced by the mobile nuclei is a faster decreasing of the mobility, i. e., the transition to the dimer regime occurs for smaller d/a ratio. In fact, since the change from one regime to the other is smooth, there is no real phase transition, but a crossover between two regimes.

D. Energy

The last quantitative result which can help study the existence of the polaron is its energy. Our interest is focused in two magnitudes: the contribution of the energy to the ion chain and the energy change due to the polaron.

The first one can be identified as the chemical potential of the impurity, which will be computed as the difference between the total energy of the system and the energy of N ions in the harmonic trap with no impurity:

$$\mu = E(N,1) - E(N,0) \tag{39}$$

where the energy function $E(N, N_{imp})$ is defined as the energy of a system composed of N ions and N_{imp} impurities.

The energy of the polaron is computed by comparing this energy to the energy of a single dimer made of an ion and the impurity in the presence of the harmonic potential. This difference should show how the distortion of the ions nearby is translated to their energy.

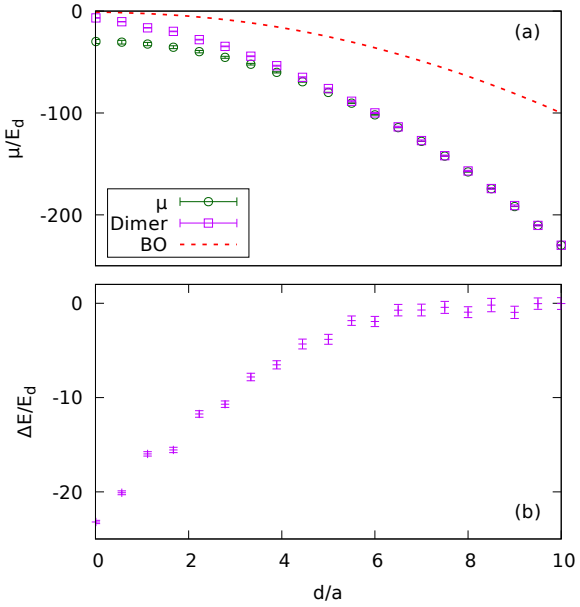

FIG. 10: (a) Chemical potential of the impurity and the same magnitude for a single dimer in the ion chain, along with the chemical potential for pinned ions (red dashed line). (b) Energy of the polaron.

The results for a mass ratio $M/m = 1$ are shown in FIG. 10. The chemical potential of the impurity is interesting from a experimental point of view as well, since this is the energy that may be obtained in an experiment. The polaron energy shows that indeed there is decrease of the energy due to the presence of the polaron, which reinforces the idea of its existence. Moreover, from both energies it can be seen that the energy of the system converges to the energy of the dimer for small scattering lengths.

Last, we want to study the effect of the parameters chosen for the trapping potential. The longitudinal oscillator length cannot be taken much larger due to the stability of the system discussed in a previous section, but one could check if there is any significant change when taking a spherical shape for oscillators, i.e. $a_x = a_y = a_z = d/10$.

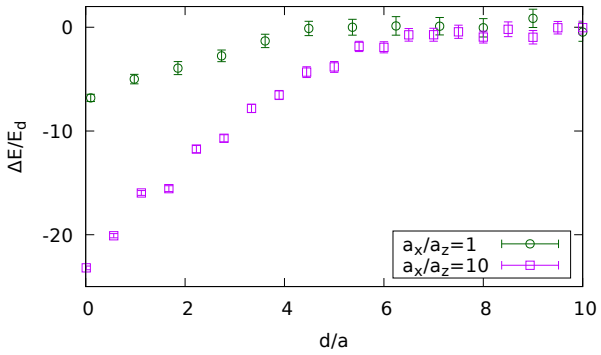

FIG. 11: Energy of the polaron for the pancake ($a_x/a_z = 10$) and spherical ($a_x/a_z = 1$) geometries of the nuclei.

The energy of the polaron for this geometry is shown in FIG. 11 along with the same magnitude computed for the pancake-like geometry. This results shows that, if the transverse trapping potential is too strong, the effect of the polaron decreases substantially, since almost all of its effect is due to the deformation in that direction. In fact, although it has not been shown in this report, the deformation diagram shown in FIG. 8 changes drastically for this spherical case: the deformation can be barely appreciated.

VII. CONCLUSIONS

To sum up, in this work we have shown the existence of polarons in a simple system made of an ion chain, which is a close representation of the original lattice where polarons were first proposed by Lev Landau. Two regimes have been found, depending on the scattering length. For small scattering lengths as compared to the lattice spacing, the impurity forms a strong bound state with one of the ions and does not interact with the rest of them. This regime has been called the dimer regime. On the other hand, in the polaron regime, for larger scattering lengths, the presence of the polaron gives rise to a transverse distortion of the nearby ions and to an energy reduction as compared to the case of a single dimer in the chain. An crucial difference, is that the polaron diffuses along the chain, while the dimer stays localized around one of the ions. However, no real phase transition has been found, but rather a crossover between these two regimes.

On the other hand, the basis of the Diffusion Monte Carlo algorithm have been studied. The three algorithms have proved to follow the expected behavior when chang-

ing the time step. Moreover, the algorithms have been programed using parallel computing too, which allows us to speedup the computation and get better statistics. In this sense, the code-development has proved to be both challenging and academical, providing a deeper understanding of the method and its basis, which would not have been acquired otherwise.

Thus, the main objectives presented in the introduction have been met: the implementation and testing of the DMC code, as well as the study of the ion chain in contact with a single impurity.

However there is still more work that can be done to develop the project further. For instance, in this work we have studied the limit of heavy ions (Born Oppenheimer approximation) and the case of equal masses for the ions and the particle. However, it might be interesting to check what is the response of the system in the opposite regime, when the ions are lighter than the impurity. Although this would be not possible in a usual solid, there is no such restriction in optical lattices. Another experiment that could be tried is to introduce some more impurities in the system, and study the full many body problem. This should be interesting because it would be a closer representation of possible experimental setup.

Acknowledgments

First of all I would like to thank my advisor Grigori for helping me develop this project during this whole year. I am so grateful to Carlos Lobo, for accepting to work with me and for every fruitful discussion. To each and every one of my classmates for the time spent together. Specially I would like to thank Joan and Sergi for all the time we have spent working side by side. Last but definitely not least, I want to thank Zabalo, for every hour we have spent working together, having fun together, and of course, for all those crazy-late-night-chats we've had. It has been a great pleasure.

[1] Zhihao Lan and Carlos Lobo. Optical lattices with large scattering length: Using few-body physics to simulate an electron-phonon system. *Physical Review A*, 90(3):033627, 2014.

[2] Immanuel Bloch, Jean Dalibard, and Wilhelm Zwerger. Many-body physics with ultracold gases. *Reviews of modern physics*, 80(3):885, 2008.

[3] Lev Davidovich Landau. Electron motion in crystal lattices. *Phys. Z. Sowjet.*, 3:664, 1933.

[4] Mark I Dykman and Emmanuel I Rashba. The roots of polaron theory. *Physics Today*, 68(4):10, 2015.

[5] Fabian Grusdt, Gregory E Astrakharchik, and Eugene Demler. Bose polarons in ultracold atoms in one dimension: beyond the fröhlich paradigm. *New Journal of Physics*, 19(10):103035, 2017.

[6] L. Parisi and S. Giorgini. Quantum monte carlo study of the bose-polaron problem in a one-dimensional gas with contact interactions. *Phys. Rev. A*, 95:023619, Feb 2017.

[7] G. E. Astrakharchik and M. D. Girardeau. Exact ground-state properties of a one-dimensional coulomb gas. *Phys. Rev. B*, 83:153303, Apr 2011.

[8] J Boronat and J Casulleras. Monte carlo analysis of an interatomic potential for he. *Physical Review B*, 49(13):8920, 1994.

[9] Kerson Huang and C. N. Yang. Quantum-mechanical many-body problem with hard-sphere interaction. *Phys. Rev.*, 105:767–775, Feb 1957.

[10] Hans Bethe and Rudolf Peierls. Quantum theory of the diplon. *Proceedings of the Royal Society of London. Series A-Mathematical and Physical Sciences*, 148(863):146–156, 1935.

[11] WMC Foulkes, L Mitas, RJ Needs, and G Rajagopal. Quantum monte carlo simulations of solids. *Reviews of Modern Physics*, 73(1):33, 2001.

[12] Arne Lüchow. Quantum monte carlo methods. *Wiley Interdisciplinary Reviews: Computational Molecular Science*, 1(3):388–402, 2011.

[13] Imran Khan and Bo Gao. Variance minimization variational monte carlo method. *arXiv preprint physics/0701223*, 2007.

[14] PRC Kent, RJ Needs, and G Rajagopal. Monte carlo energy and variance-minimization techniques for optimizing many-body wave functions. *Physical Review B*, 59(19):12344, 1999.

[15] CJ Umrigar, KG Wilson, and JW Wilkins. Optimized trial wave functions for quantum monte carlo calculations. *Physical Review Letters*, 60(17):1719, 1988.

[16] Angelo Corana, Michele Marchesi, Claudio Martini, and Sandro Ridella. Minimizing multimodal functions of continuous variables with the "simulated annealing". *ACM Transactions on Mathematical Software (TOMS)*, 13(3):262–280, 1987.

[17] Ioan Kosztin, Byron Faber, and Klaus Schulten. Introduction to the diffusion monte carlo method. *American Journal of Physics*, 64(5):633–644, 1996.

[18] Peter J Reynolds, David M Ceperley, Berni J Alder, and William A Lester Jr. Fixed-node quantum monte carlo for moleculesa) b). *The Journal of Chemical Physics*, 77(11):5593–5603, 1982.

[19] Tao Pang. *An Introduction to Computation Physics*. University Press, Cambridge, 2006.

[20] CJ Umrigar, MP Nightingale, and KJ Runge. A diffusion monte carlo algorithm with very small time-step errors. *The Journal of chemical physics*, 99(4):2865–2890, 1993.

[21] Siu A Chin. Quadratic diffusion monte carlo algorithms for solving atomic many-body problems. *Physical Review A*, 42(12):6991, 1990.

[22] A Sarsa, J Boronat, and J Casulleras. Quadratic diffusion monte carlo and pure estimators for atoms. *The Journal of chemical physics*, 116(14):5956–5962, 2002.

[23] Jon Kristian Nilsen. Montepython: Implementing quantum monte carlo using python. *Computer Physics Communications*, 177(10):799–814, 2007.